applied sciences

MDPI

Article

CPM-GFDM: A Novel Combination of Continuous Phase Modulation and Generalized Frequency Division Multiplexing for Wireless Communication

Imran A. Tasadduq

Department of Computer Engineering, Umm Al-Qura University, Makkah 21955, Saudi Arabia; iatasadduq@uqu.edu.sa

Abstract: In this paper, continuous phase modulation-generalized frequency division multiplexing (CPM-GFDM) is proposed. The performance of CPM-GFDM is evaluated over Gaussian and frequency selective fading channels. In the proposed technique, the mapper in the transmitter and the de-mapper in the receiver of traditional GFDM are replaced by a CPM mapper and de-mapper, respectively. Using Monte-Carlo simulations, the bit error rate performance is evaluated for several rational values of the modulation index. We establish the superiority of CPM-GFDM over traditional GFDM using error performance plots through extensive simulations. We demonstrate that there are several values of the modulation index that give a performance superior to the conventional GFDM, with $h = \frac{1}{2}, \frac{3}{10}, \frac{5}{16}, \frac{7}{16}$ giving the best performance for additive white Gaussian noise (AWGN) channels, while for the frequency-selective channels the best performance is observed when $h = \frac{3}{10}, \frac{5}{16}, \frac{7}{16}$.

Keywords: CPM; continuous phase modulation; GFDM; generalized frequency division multiplexing; bit error rate

Citation: Tasadduq, I.A. CPM-GFDM: A Novel Combination of Continuous Phase Modulation and Generalized Frequency Division Multiplexing for Wireless Communication. *Appl. Sci.* **2023**, *13*, 854. https://doi.org/10.3390/app13020854

Academic Editors: Paulo M. Mendes, Jose Cabral and Hugo Daniel da Costa Dinis

Received: 27 November 2022
Revised: 29 December 2022
Accepted: 4 January 2023
Published: 7 January 2023

1. Introduction

There are several contenders for 5G communication. Some of them are filter bank multicarrier (FBMC), universal filtered multicarrier (UFMC) [1–3], non-orthogonal multiple access (NOMA) [4,5], filtered orthogonal frequency division multiplexing (f-OFDM) [6] and generalized frequency division multiplexing (GFDM) [7]. Out of these, GFDM, which is a non-orthogonal modulation technique, adequately addresses the shortcomings of OFDM for the next generation of 5G networks [7]. Its benefits include flexibility, minimal out-of-band (OOB) emissions, and a higher spectrum efficiency [8]. A heterogeneous network with a variety of competing technologies, such as D2D communication, millimeter waves, multiple input multiple output (MIMO), massive MIMO, femtocells, and Pico cells is anticipated for 5G [9]. To lessen OOB emissions, each GFDM data-block is broken up into subcarriers and sub-symbols, with the subcarriers being filtered by a pulse shaping filter. With its capacity to work with single carrier, FBMC and frequency domain systems that are based on equalization, GFDM is a very flexible time-frequency distribution technique [10]. As GFDM is block-based, it can use several OFDM techniques, including cyclic prefix (CP), to prevent inter-symbol interference. Thus, to mitigate the impacts of multipath at the receiver side, low complexity equalizers can be used in the frequency domain [11]. The loss of orthogonality that results from GFDM subcarriers being filtered via a range of pulse shapes [12] makes them vulnerable to self-interference at the receiver. The resulting complexity in implementation is another drawback of using the flexible waveform. However, since reducing the complexity of systems is an active area of research and computer power is increasing quickly, GFDM turns out to be a promising technique for upcoming high-speed, high performance communications.

While several authors have focused on reducing the complexity of the GFDM receiver (see, for example, [13,14]), or minimizing the interference [11,15–17], some others have focused on presenting an analysis of BER when using some novel technique in GFDM [18–21].

Channel codes have also been used to improve the BER of GFDM [22]. MIMO-GFDM is an active research area which has been employed to improve the BER of a conventional GFDM system. For example, improvement in spectral efficiency and BER via MIMO-GFDM has been proposed in [23]. Low-complexity receivers for MIMO-GFDM have been proposed in [24,25]. There are several other papers that try to improve the performance of GFDM and/or MIMO-GFDM by using novel techniques, for example, [10,26–28]. However, only a handful of work exists that focuses on improving the performance by modifying mapping schemes (one such example is [29]).

CPM and its subclass, continuous phase frequency shift keying (CPFSK), have been well established in communication systems for more than 40 years [30]. These systems' key benefits are the signal's power and spectrum efficiency, consistent envelope, low levels of out-of-band radiation, flexibility, and phase continuity [31–33]. One of the factors driving the development of the 5G architecture, which includes enhanced mobile broadband, machine type communication (MTC), and ultra-reliable MTC, is flexibility [34,35]. In the mapper of traditional GFDM, memoryless modulation techniques such as PSK and QAM are used. A thorough literature search suggests there has been no work that integrates CPM in the mapper of a GFDM. Our main goal in this work is to improve the BER performance of a GFDM by using CPM as a mapper.

The remaining paper is organized in the following manner. Section 2 presents the details of proposed CPM-GFDM Tx-Rx that comprises CPM modulator and demodulator. Simulation setup and results are presented in Section 3, followed by a discussion in Section 4. The paper is concluded in Section 5.

2. Proposed CPM-GFDM Transceiver

This section presents the proposed CPM-GFDM transmitter and receiver.

2.1. CPM-GFDM Transmitter

The proposed CPM-GFDM transmitter is shown in Figure 1. As shown in this figure, data bits go through the CPM mapper to become converted into CPM-mapped complex numbers, followed by upsampling. Then, M symbols are collected followed by the pulse shaping filter and IFFT. Cyclic prefix is added next, and the signal is transmitted.

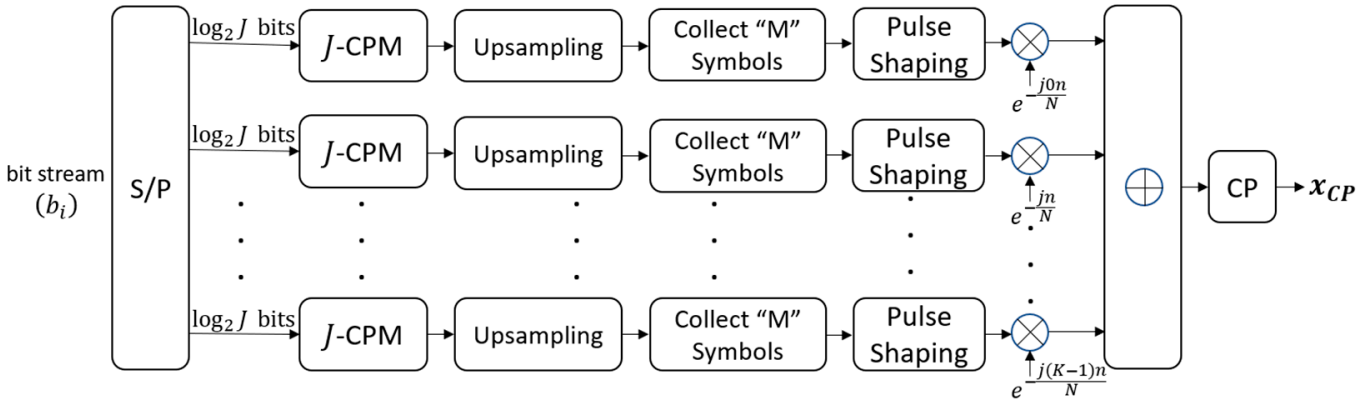

Figure 1. Proposed CPM-GFDM Transmitter.

Let K represent the number of subcarriers and let M represent the number of symbols in each subcarrier. A serial bit stream b_i is converted into a parallel stream of K symbols where each symbol contains $\log_2 J$ bits feeding J-CPM mappers. These mappers produce J-ary CPM-modulated complex-valued data symbols at their outputs. The next block upsamples the complex symbol sequence by a factor of N where N number of samples are used to represent a time slot. These operations repeat until M symbols—denoted by a vector $\bar{d}_k$ where $k = 0, 1, \ldots, K-1$—are received at each subcarrier, with $\bar{d}_k = [d_{k,0}, d_{k,1}, \ldots, d_{k,M-1}]$. Therefore, each of the K subcarriers transmits M complex-valued data symbols per GFDM

frame. Hence, the transmitted signal will consist of $K \times M$ data symbols that could be represented by a matrix $\boldsymbol{d}$ as shown below [36]:

$$\boldsymbol{d} = \begin{bmatrix} \overline{d}_0 \\ \vdots \\ \overline{d}_{K-1} \end{bmatrix}$$

or

$$\boldsymbol{d} = \begin{bmatrix} d_{0,0} & d_{0,1} & \dots & d_{0,M-1} \\ d_{1,0} & \ddots & & d_{1,M-1} \\ \vdots & & \ddots & \vdots \\ d_{K-1,0} & d_{K-1,1} & \dots & d_{K-1,M-1} \end{bmatrix} \tag{1}$$

The kth row in the aforementioned matrix denotes the data symbols sent over the kth subcarrier, and the mth column denotes the data symbols sent over the mth time slot. Each of the elements in this matrix has been modulated by CPM and is given by:

$$d_{k,m} = \cos \phi_k[l] + j \sin \phi_k[l] \tag{2}$$

where l represents the present symbol index, and the information-bearing phase $\phi_k[l]$ for the kth subcarrier is given by:

$$\phi_k[l] = \pi \sum_{i=-\infty}^{l-1} h_k[i]\alpha_k[i] + \pi h_k[l]\alpha_k[l] \tag{3}$$

$\{\alpha_k[i]\}$ denotes the sequence of J-ary information-carrying symbols for the kth subcarrier and ith symbol that belong to the set $\pm 1, \pm 3, \dots, \pm(J-1)$, $\alpha_k[l]$ is the present symbol for the kth subcarrier, and $\{h_k[i]\}$ for the kth subcarrier and ith symbol are called modulation indices. If $\forall i,\ h_k[i] = h_k$, this indicates that h is the same for all symbols for kth subcarrier. This scheme is typically known as "single h" CPM. If the value of h is different from symbol to symbol, then this type of CPM is known as "multi-h" CPM. In multi-h CPM, the value of $\{h_k[i]\}$ changes in a round robin fashion out of all the h values. In this work, we use single h CPM and an identical modulation index for all the subcarriers. The most advantageous aspect of a CPM scheme is that it has memory, which is symbolized by the first term in (3). It is obvious that all symbols up to $(l-1)$ symbols are added together to make up the phase $\phi_k[l]$ [37,38].

Let p and q be two relatively prime integers. Then, the modulation index h is chosen as the ratio of p and q such that $0 < h < 1$. By doing so, catastrophic phase situations are prevented and the overall number of points in the CPM constellation are limited to a manageable level [39]. The phase states for even p are given as,

$$\phi_k = \left\{ 0, \pi\frac{p}{q}, 2\pi\frac{p}{q}, \dots, (q-1)\pi\frac{p}{q} \right\} \tag{4}$$

On the other hand, the phase states ϕ_k for odd p are given as,

$$\phi_k = \left\{ 0, \pi\frac{p}{q}, 2\pi\frac{p}{q}, \dots, (2q-1)\pi\frac{p}{q} \right\} \tag{5}$$

The signal constellation has q points when p is even, and $2q$ when p is odd, as shown by (4) and (5), respectively. For instance, the signal constellation has five possible points if for a binary CPM, $h = \frac{2}{5}$, as seen below and shown in Figure 2:

$$\phi_k = \left\{ 0, \frac{2\pi}{5}, \frac{4\pi}{5}, \frac{6\pi}{5}, \frac{8\pi}{5} \right\} \tag{6}$$

and eight possible points if $h = \frac{1}{4}$, as shown below and shown in Figure 2:

$$\phi_k = \left\{0, \frac{\pi}{4}, \frac{\pi}{2}, \frac{3\pi}{4}, \pi, \frac{5\pi}{4}, \frac{3\pi}{2}, \frac{7\pi}{4}\right\} \tag{7}$$

Figure 2. Constellation example for a binary CPM (**a**) $h = 2/5$ (**b**) $h = 1/4$.

Next, a pulse shaping filter—denoted by $g[n]$—is applied. This is a circular prototype filter whose length is $N \times M$ for a kth subcarrier since each subcarrier carries N samples per symbol and there are M symbols at each subcarrier. For each subcarrier k, the filter is delayed by mN in time corresponding to the mth symbol where $m = 0, 1, \ldots, M-1$. Five pulse shaping circular filters have been investigated in the literature. These are: (1) Root Raised Cosine, (2) Raised Cosine, (3) Xia Pulse, (4) Gaussian Pulse, and (5) Dirichlet Pulse [40].

The pulse shaping filter is followed by IFFT, which is essentially an up-conversion of the complex stream by a complex subcarrier. Hence, the transmitted signal $x[n]$, without the cyclic prefix, is given by

$$x[n] = \sum_{m=0}^{M-1} \sum_{k=0}^{K-1} d_{k,m} g([n - mN]_{NM}) e^{-j2\pi k \frac{n}{N}} \tag{8}$$

The above equation can be represented in the form of a matrix as in [36]

$$\boldsymbol{x} = \boldsymbol{AD} \tag{9}$$

where

$$\boldsymbol{A} = \begin{bmatrix} g[n] \\ g[n]e^{-j2\pi\frac{n}{N}} \\ \vdots \\ g[n]e^{-j2\pi(K-1)\frac{n}{N}} \\ g[n-N] \\ g[n-N]e^{-j2\pi\frac{n}{N}} \\ \vdots \\ g[n-N]e^{-j2\pi(K-1)\frac{n}{N}} \\ \vdots \\ \vdots \\ g[n-(M-1)N] \\ g[n-(M-1)N]e^{-j2\pi\frac{n}{N}} \\ \vdots \\ g[n-(M-1)N]e^{-j2\pi(K-1)\frac{n}{N}} \end{bmatrix}^T$$

$$\boldsymbol{D} = \begin{bmatrix} d_{0,0} \\ d_{1,0} \\ \vdots \\ d_{K-1,0} \\ d_{0,1} \\ d_{1,1} \\ \vdots \\ d_{K-1,1} \\ \vdots \\ \vdots \\ d_{0,M-1} \\ d_{1,M-1} \\ \vdots \\ d_{K-1,M-1} \end{bmatrix}$$

The transmitted signal after adding the CP can be expressed as in [41]

$$\boldsymbol{x_{CP}} = \begin{bmatrix} \boldsymbol{x}(NM - N_{CP} + 1 : NM) & \boldsymbol{x} \end{bmatrix} \tag{10}$$

where N_{CP} represents the CP samples.

2.2. CPM-GFDM Receiver

2.2.1. Received Signal and the Channel

The received signal can be represented in matrix form as

$$\boldsymbol{r} = \boldsymbol{H}\boldsymbol{x_{CP}} + \boldsymbol{n} \tag{11}$$

where $\boldsymbol{H}$ is the channel matrix and $\boldsymbol{n}$ is the additive white Gaussian noise with zero mean and σ^2 variance. The proposed CPM-GFDM receiver is shown in Figure 3. After removing the CP, the received signal goes through the equalizer, assuming known $\boldsymbol{H}$. The equalization can be expressed mathematically as in [42]

$$\boldsymbol{r_{eq}} = \boldsymbol{H}^{-1}\boldsymbol{HAD} + \boldsymbol{H}^{-1}\boldsymbol{n} = \boldsymbol{AD} + \widetilde{\boldsymbol{n}} \tag{12}$$

where $\widetilde{\boldsymbol{n}}$ represents the colored noise.

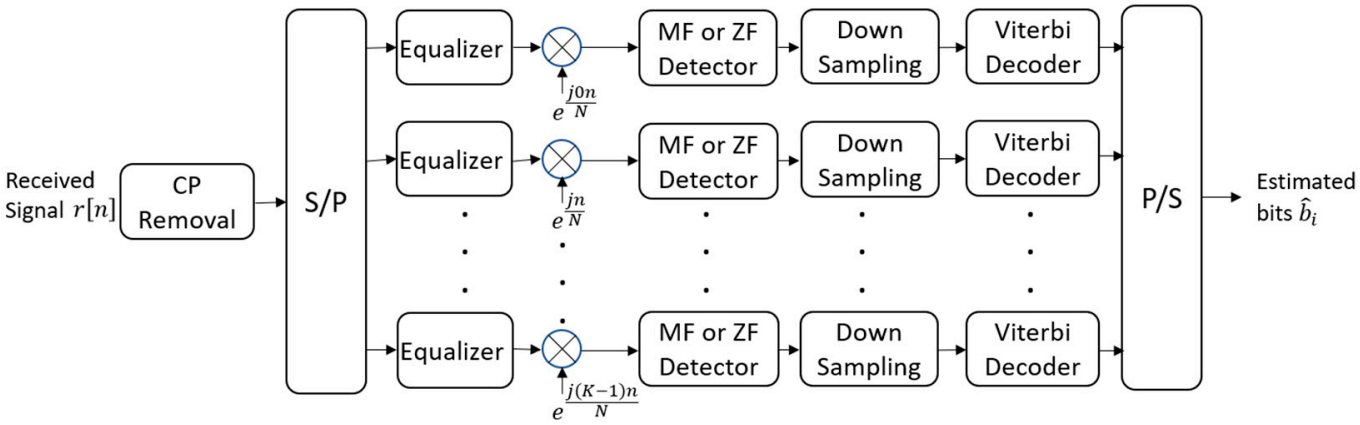

Figure 3. Proposed CPM-GFDM Receiver.

2.2.2. GFDM Demodulator

Next, FFT is taken. This is followed by one of the three types of GFDM receivers—matched filter (MF), zero forcing (ZF), or minimum mean square error (MMSE). In this work, we explore MF and ZF. Pre-multiplying (8) by a square matrix Z having $KM \times KM$ dimensions, we obtain

$$Z\boldsymbol{r_{eq}} = Z\boldsymbol{AD} + Z\tilde{\boldsymbol{n}} \tag{13}$$

The matrix Z is computed such that the estimated transmitted data symbols $\hat{\boldsymbol{D}}$ can be obtained as

$$\hat{\boldsymbol{D}} = Z\boldsymbol{r_{eq}} \tag{14}$$

The method of computing the Z matrix determines whether a matched filter or a zero-forcing receiver is being employed, which is discussed next.

2.2.3. Matched Filter Receiver

The receiver is known as a matched filter receiver if Z is specified to be $\boldsymbol{A}^H$ in (14), where H indicates Hermitian. This kind of receiver would increase the SNR for each subcarrier at the expense of producing self-interference in the event that the transmitter uses a non-orthogonal pulse.

2.2.4. Zero Forcing Receiver

For this particular receiver, $Z = \boldsymbol{A}^{-1}$. In case $\boldsymbol{A}$ is not square, its pseudo-inverse, $\boldsymbol{A}^+$, is computed using the following relationship:

$$\boldsymbol{A}^+ = \left(\boldsymbol{A}^H\boldsymbol{A}\right)^{-1}\boldsymbol{A}^H \tag{15}$$

where $\boldsymbol{A}^H$ is the Hermitian of $\boldsymbol{A}$. A zero forcing receiver reduces self-interference but amplifies noise.

2.2.5. Viterbi Decoder

After down sampling, the signal goes to CPM signal detection block. CPM detection is complex. The complexity can be reduced if we use a Viterbi Decoder (VD) [43]. If h is rational—the CPM trellis has a reasonable number of states. This facilitates the use of VD.

With reference to Figure 4, we demonstrate the angle ϕ_k, the associated complex numbers, and the paths that the data sequence 10011 takes through the trellis (shown with red colored lines) for a given subcarrier when $h = 2/5$. To start with, we assume state $\phi_k = 0$ $(d_{k,m} = 1 + j0)$. If the next bit is a one (indicated by a solid line), the state changes to $0 + \frac{2\pi}{5} = \frac{2\pi}{5}$. On the other hand, if the next bit is a zero, (indicated by a dashed line), the state changes to $0 - \frac{2\pi}{5} = -\frac{2\pi}{5} = \frac{8\pi}{5}$. This trend continues deep into the trellis. Consequently, we can trace a particular path based on the data sequence, as has also been shown in Figure 4.

VD computes the distance between the incoming signal and all trellis routes entering each state at a given moment i. The paths that are most likely not the candidates for maximum likelihood are then eliminated. The "surviving path" is the path that is chosen when two paths enter the same state; it is the path with the best metric. Similar surviving paths are chosen for all the states. By carrying on in the same way, VD moves further into the trellis and decisions are determined by eliminating the least likely paths [44]. Despite not being maximum likelihood in the strictest sense, these decisions can be almost as excellent as in the maximum likelihood case if the decision depth is sufficient [45].

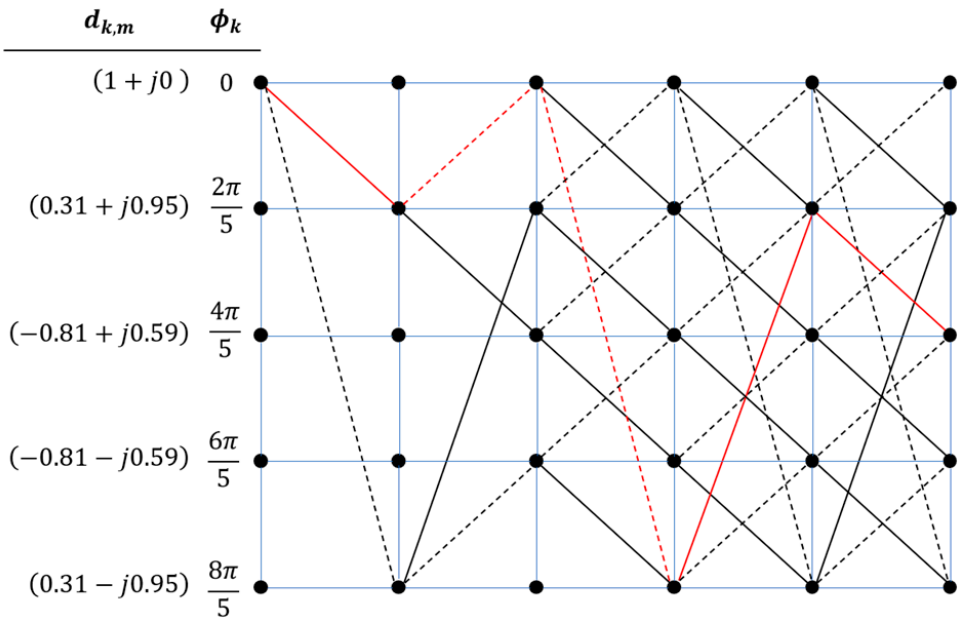

Figure 4. The Viterbi decoder for a typical example with $h = 2/5$. Bit 1 is indicated by solid lines while bit 0 is indicated by broken lines. The bit sequence 10011 is shown using red colored lines. The outputs of the CPM mapper are shown using the complex numbers under $d_{k,m}$.

In the following, we demonstrate the method to compute the distance between the received bit sequence and the possibly received sequences. At the output of FFT, $\hat{d}_{k,m}$ denotes the received complex numbers at subcarrier k. Additionally, let a typical complex number from the received sequence be represented as

$$\hat{d}_{k,m} = \hat{u}_{k,m} + j\hat{v}_{k,m}$$

Let a typical complex number from the transmitted sequence be

$$d_{k,m} = u_{k,m} + jv_{k,m}$$

In the above equation, real parts are $\hat{u}_k$ and u_k for the received and transmitted complex numbers, respectively. Similarly, the imaginary parts are $\hat{v}_k$ and v_k for the received and transmitted complex numbers, respectively. Using $s_{k,m}$ to denote the square of the distance between two complex numbers, $s_{k,m}$ can be computed as

$$s_{k,m} = (u_{k,m} - \hat{u}_{k,m})^2 + (v_{k,m} - \hat{v}_{k,m})^2 \tag{16}$$

These distances are successively updated at each symbol interval. All potential state transitions are also expanded. At the following symbol interval, the path with the highest likelihood is kept while the rest are eliminated. All competitors conclude at the trellis's most extreme end after tracing the entire signal sequence. As a result, the sequence that is required is the one that is the most likely to occur. VD only records q or $2q$ states at each time interval because h is the ratio of p and q, which are relatively prime. The VD provides a judgment on the complete sequence of w symbols at the end of w symbol intervals if w indicates the decision depth in terms of the number of symbols.

3. Numerical Results

In this section, we present the numerical results on the bit error rate (BER) performance of the proposed CPM-GFDM system for various values of h. Our simulations are based on the Matlab code available on the Vodafone Chair website [46]. We consider two channels, namely the additive white Gaussian noise (AWGN) channel and a frequency-selective channel. Moreover, we compare the performance achieved by the proposed system with PSK-GFDM and QAM-GFDM. The GFDM parameters used for the simulations are listed in Table 1, while the modulation indices (h) used for the CPM mapper are shown in Table 2. By changing the numerator p from 1 to 15, we were able to choose the values for the modulation index h. To ensure that p/q remained rational, we varied the denominator q's values from 2 to 16. There are 23 different values of h as a result. We concluded that this set of variables is sufficient to assess the performance of CPM-GFDM because any other numbers that are outside of this range do not produce results that are any better than the ones produced by rational values of h. Additionally, using higher p and q numbers would increase the number of points in the constellation, which would result in a complex VD.

Table 1. GFDM Parameters.

Parameters	Value
No. of subcarriers (K)	128
No. of sub-symbols per subcarrier (M)	5
No. of active subcarriers (Kon)	128
No. of active sub-symbols (Mon)	5
Cyclic prefix (CP)	32
Roll off factor (α)	0.5
Pulse shape	RRC
Mapper	QAM, PSK, CPM
Sampling rate	10 MHz

Table 2. CPM Modulation Indices.

No.	p	q	$h=\frac{p}{q}$
1	1	2	0.5
1	1	4	0.25
2	1	5	0.2
3	1	8	0.125
4	1	10	0.1
5	1	16	0.0625
6	2	5	0.4
7	3	4	0.75
8	3	5	0.6
9	3	8	0.375
10	3	10	0.3
11	3	16	0.1875
12	4	5	0.8
13	5	8	0.625

Table 2. *Cont.*

No.	p	q	$h=\frac{p}{q}$
14	5	16	0.3125
15	6	10	0.6
16	7	8	0.875
17	7	10	0.7
18	7	16	0.4375
19	9	10	0.9
20	9	16	0.5625
21	11	16	0.6875
22	13	16	0.8125
23	15	16	0.9375

3.1. Power Spectral Density

One of the main disadvantages of OFDM is its high out-of-band (OOB) radiation, which is mainly due to the rectangular pulse [47,48]. Due to high OOB, the symbols would interact with neighboring channels. As a result, OFDM is not considered suitable for 5G communication. The OOB radiation of the broadcast signal for the 5G base stations must be below the necessary limitations, i.e., −45 dB, to satisfy the spectrum regulatory masks [49]. GFDM is known to have lower OOB radiation as compared to OFDM [40,50,51]. This is mainly due to the fact that a prototype filter that is circularly shifted in both the time and frequency domains shapes the data symbols [49]. Figure 5 shows the power spectral density (PSD) of proposed GFDM and compares it with that of conventional GFDM. It is evident from this figure that the PSD of the proposed GFDM is superior in terms of OOB radiation, as it is lower than that of the conventional GFDM.

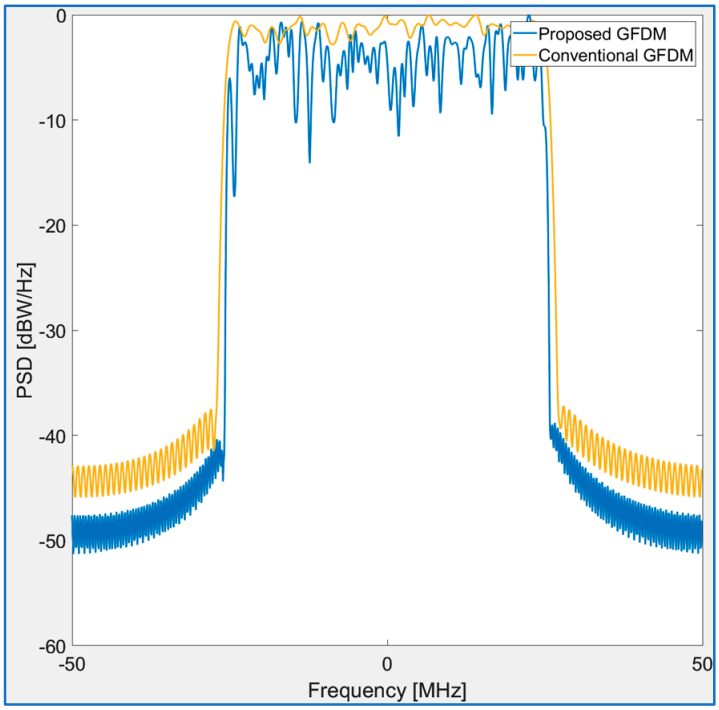

Figure 5. Power spectral density of the proposed system compared with that of the conventional system.

3.2. Performance in the AWGN Channel

Figures 6–11 show the error performance of CPM-GFDM and compare it with that of QAM-GFDM or PSK-GFDM for an AWGN channel. The error performance for a binary system is shown in Figures 6 and 7 when using matched filter receiver and zero forcing receiver, respectively. It is observed that with matched filter receiver, there are several values of h for which the proposed system outperforms the conventional GFDM, with $h = 1/2$ giving the best performance. Table 4 identifies those values of h that outperform conventional GFDM. However, when using zero forcing receiver, there is no value of h that beats the conventional GFDM, the closest being $h = 3/5,\ 5/8,\ 9/16$.

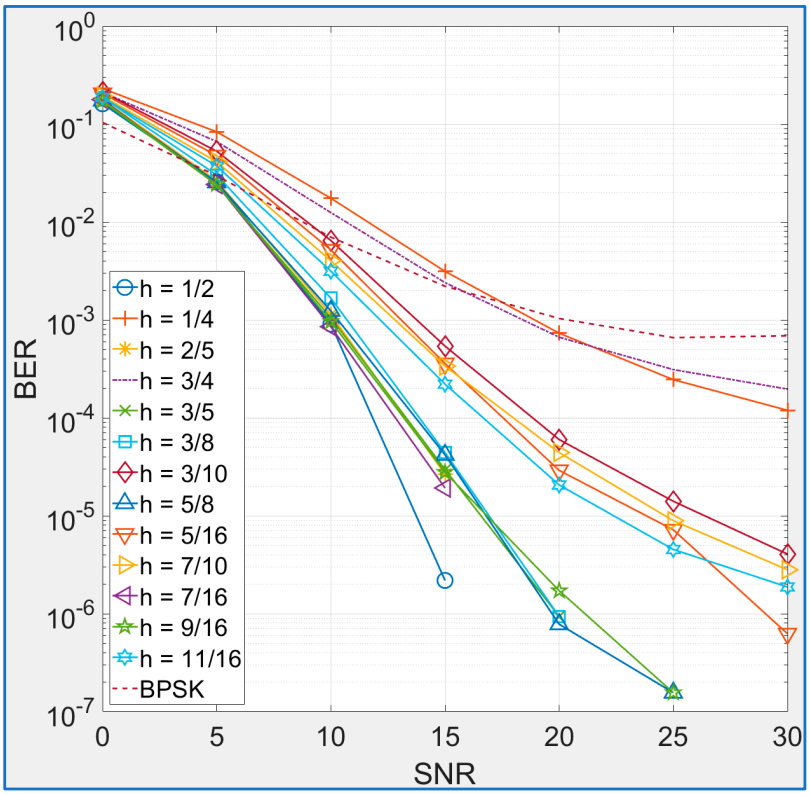

Figure 6. BER performance of binary CPM-GFDM vs. BPSK-GFDM for matched filter receiver over AWGN channels.

The error performance of CPM-GFDM against QAM-GFDM when using two bits at a time (i.e., $J = 4$) is shown in Figures 8 and 9 for the two receivers. For the case of matched filter receiver, it is observed that there are several values of h for which the error performance of the proposed system is better than QAM-GFDM. The best performance is observed in the case when $h = 7/16$. The complete list of h values for which the proposed system outperforms QAM-GFDM is given in Table 4. When using a zero-forcing receiver, there is no value of h that performs better than QAM-GFDM. The h values that are close to QAM-GFDM when using zero forcing are $1/4$ and $3/10$.

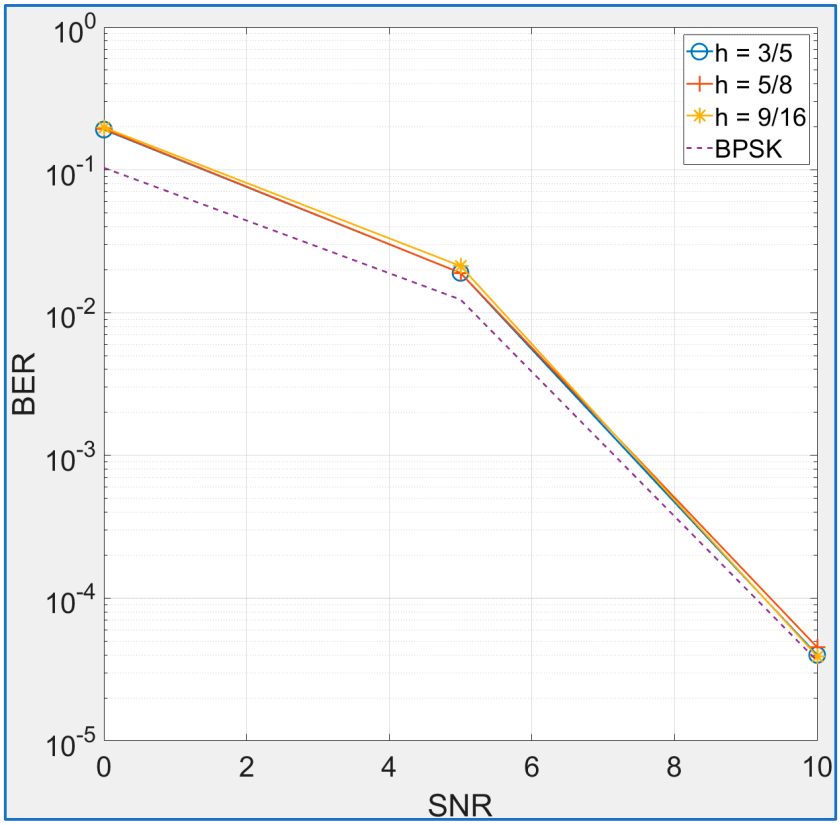

Figure 7. BER performance of binary CPM-GFDM vs. BPSK-GFDM for zero forcing receiver over AWGN channels.

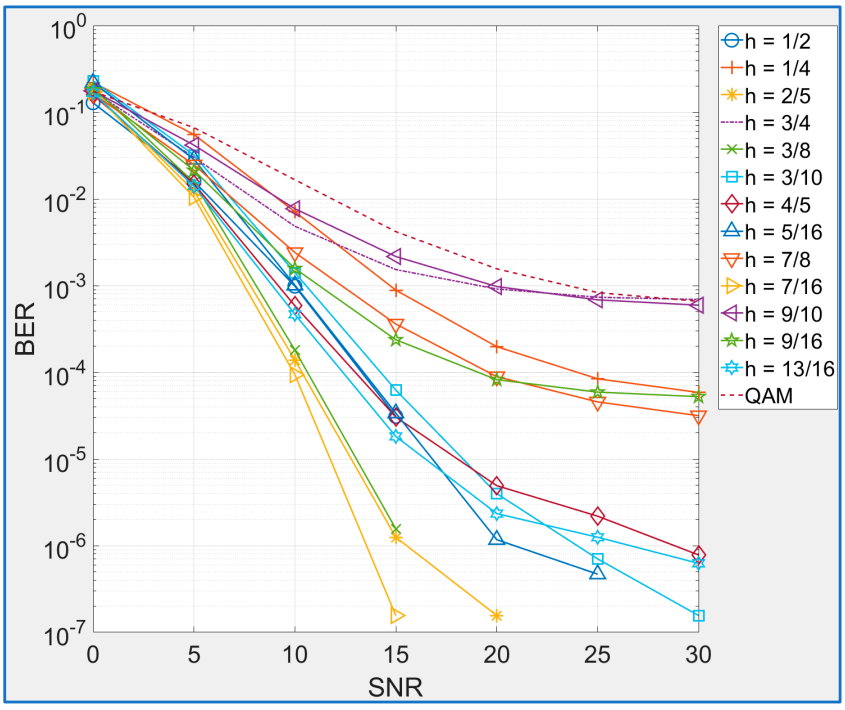

Figure 8. BER performance of CPM-GFDM vs. QAM-GFDM with $J = 4$ for matched filter receiver over AWGN channels.

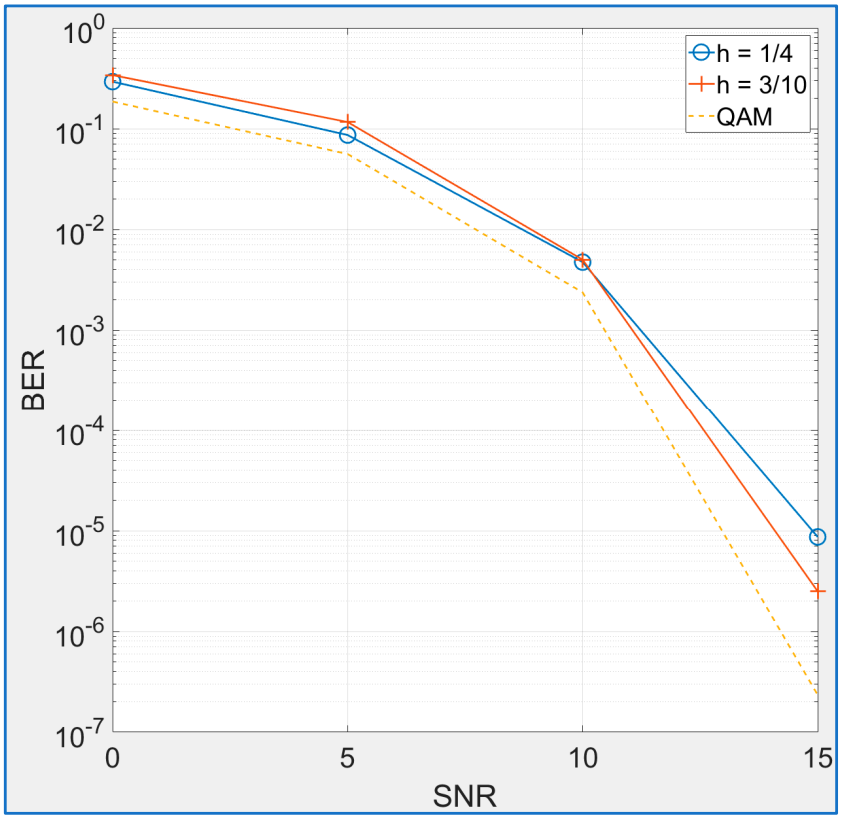

Figure 9. BER performance of CPM-GFDM vs. QAM-GFDM with $J = 4$ for zero forcing receiver over AWGN channels.

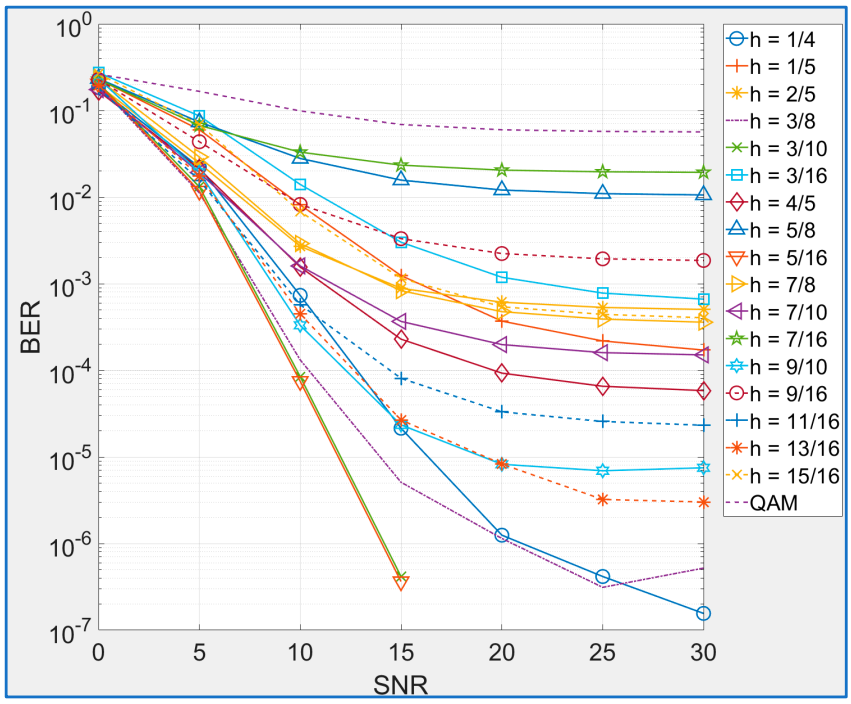

Figure 10. BER performance of CPM-GFDM vs. QAM-GFDM with $J = 8$ for matched filter receiver over AWGN channels.

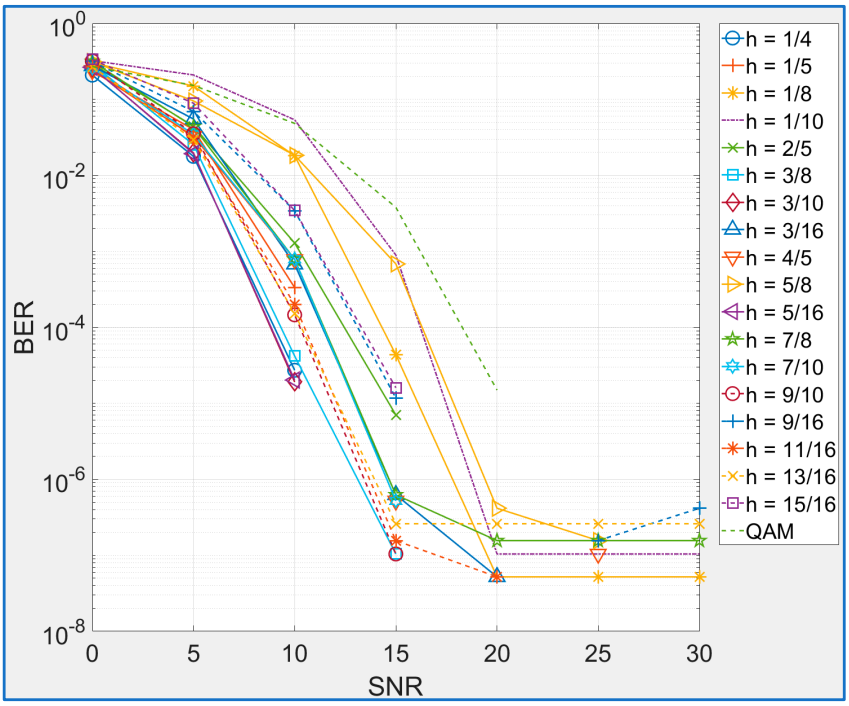

Figure 11. BER performance of CPM-GFDM vs. QAM-GFDM with $J = 8$ for zero forcing receiver over AWGN channels.

Finally, the error performance when using three bits at a time (i.e., $J = 8$) is shown in Figures 10 and 11. It is observed that, in this case, out of 23 values of h there are 17 values that give a performance better than QAM-GFDM when using a matched filter receiver. The best performance is observed in the case when $h = 5/16$ and $h = 3/10$. Moreover, as Figure 11 shows, the proposed system outperforms the conventional GFDM for 18 values of h, with the best performance observed when $h = 5/16,\ 3/10$.

3.3. Performance in Frequency-Selective Channel

As indicated in Table 3, we have chosen the ITU outdoor channel model A with six taps to produce the multipath components [52].

Table 3. Frequency-Selective Channel.

Tap	Relative Delay (ns)	Average Power (dB)
1	0	0
2	300	−1
3	700	−9
4	1100	−10
5	1700	−15
6	2500	−20

Figures 12–17 show the error performance of CPM-GFDM and compare it with that of QAM-GFDM or PSK-GFDM for the frequency-selective channel shown in Table 3. The error performance for a binary system is shown in Figures 12 and 13 when using matched filter receiver and zero forcing receiver, respectively. As was observed over the AWGN channel, in this case, as well, with the matched filter receiver, there are several values of h for which the proposed system outperforms the conventional GFDM. Table 4 identifies those values of h that outperform conventional GFDM. However, unlike the AWGN channel, the best

performance is observed when using $h = 7/16$. When using the zero-forcing receiver, there is no value of h that beats the conventional GFDM, the closest being $h = 7/16$, as has been shown in Figure 13.

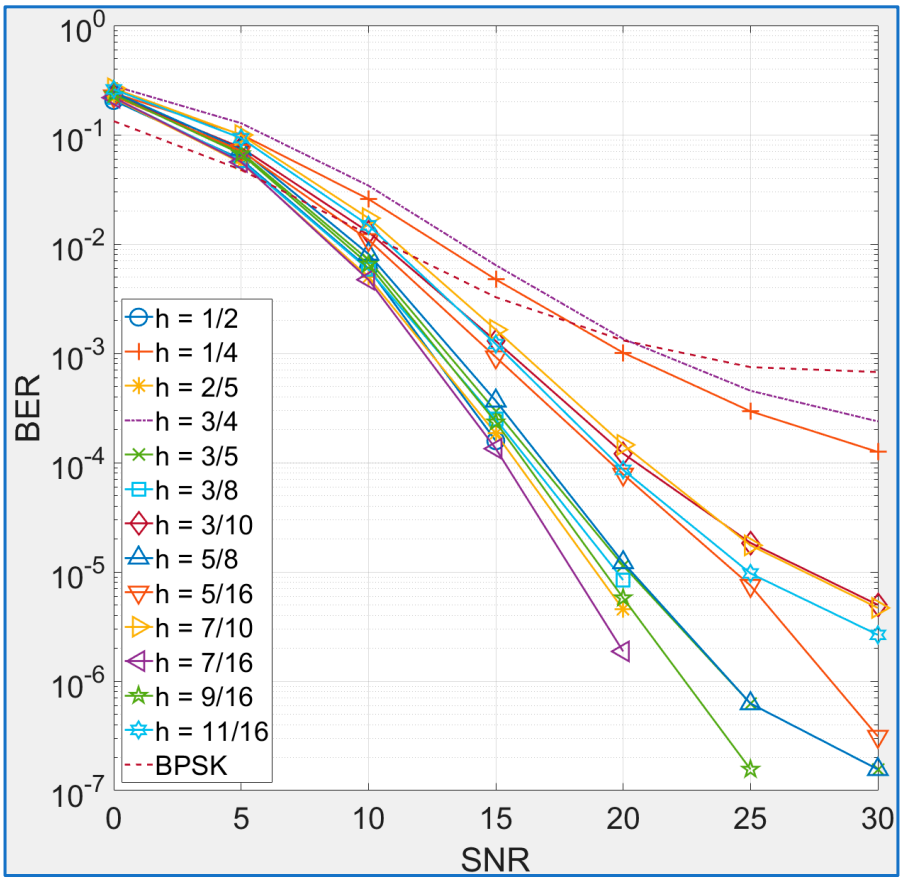

Figure 12. BER performance of binary CPM-GFDM vs. BPSK-GFDM for matched filter receiver over frequency-selective channels.

Table 4. Modulation Indices Giving Better Performance Than Conventional GFDM.

	AWGN Channel						**Frequency-Selective Channel**					
	***J*=2**		***J*=4**		***J*=8**		***J*=2**		***J*=4**		***J*=8**	
$h=\frac{p}{q}$	**MF**	**ZF**	**MF**	**ZF**	**MF**	**ZF**	**MF**	**ZF**	**MF**	**ZF**	**MF**	**ZF**
1/2	✓	-	✓	-	-	✓	✓	-	-	-	-	-
1/4	✓	-	✓	-	✓	✓	✓	-	-	✓	✓	✓
1/5	-	-	-	-	✓	✓	-	-	-	-	-	-
1/8	-	-	-	-	-	✓	-	-	-	-	-	-
1/10	-	-	-	-	-	✓	-	-	-	-	-	-
1/16	-	-	-	-	-	-	-	-	-	-	-	-
2/5	✓	-	✓	-	✓	✓	✓	-	✓	-	-	-
3/4	✓	-	✓	-	-	-	✓	-	-	-	-	-
3/5	✓	-	-	-	-	-	✓	-	-	-	-	-
3/8	✓	-	✓	-	✓	✓	✓	-	✓	-	-	-

Table 4. *Cont.*

	AWGN Channel						Frequency-Selective Channel					
	J=2		*J*=4		*J*=8		*J*=2		*J*=4		*J*=8	
$h=\frac{p}{q}$	MF	ZF	MF	ZF	MF	ZF	MF	ZF	MF	ZF	MF	ZF
3/10	✓	-	✓	-	✓	✓	✓	-	✓	✓	✓	✓
3/16	-	-	-	-	✓	✓	-	-	-	-	-	-
4/5	-	-	✓	-	✓	✓	-	-	✓	-	✓	✓
5/8	✓	-	-	-	✓	✓	✓	-	-	-	-	-
5/16	✓	-	✓	-	✓	✓	✓	-	-	✓	✓	-
7/8	-	-	✓	-	✓	✓	-	-	-	-	-	-
7/10	✓	-	-	-	✓	✓	✓	-	-	-	-	-
7/16	✓	-	✓	-	✓	-	✓	-	✓	-	-	-
9/10	-	-	✓	-	✓	✓	-	-	-	-	-	-
9/16	✓	-	✓	-	✓	✓	✓	-	-	-	-	-
11/16	✓	-	-	-	✓	✓	✓	-	-	-	-	-
13/16	-	-	✓	-	✓	✓	-	-	-	-	-	-
15/16	-	-	-	-	✓	✓	-	-	-	-	-	-

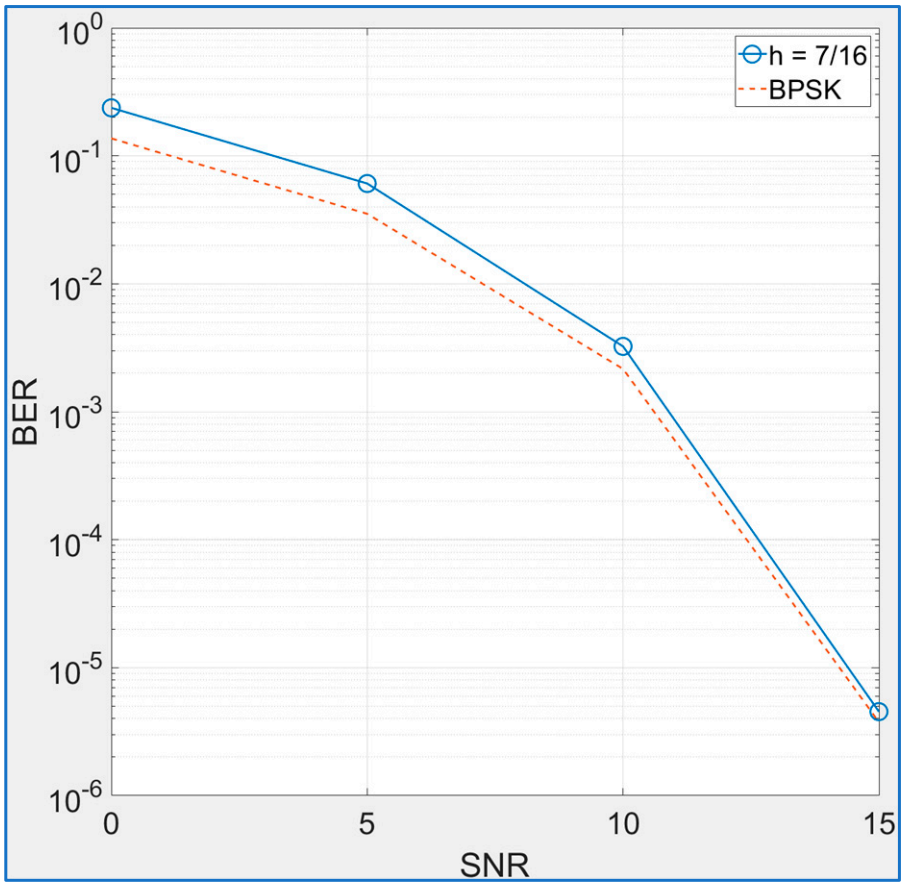

Figure 13. BER performance of binary CPM-GFDM vs. BPSK-GFDM for zero forcing receiver over frequency-selective channels.

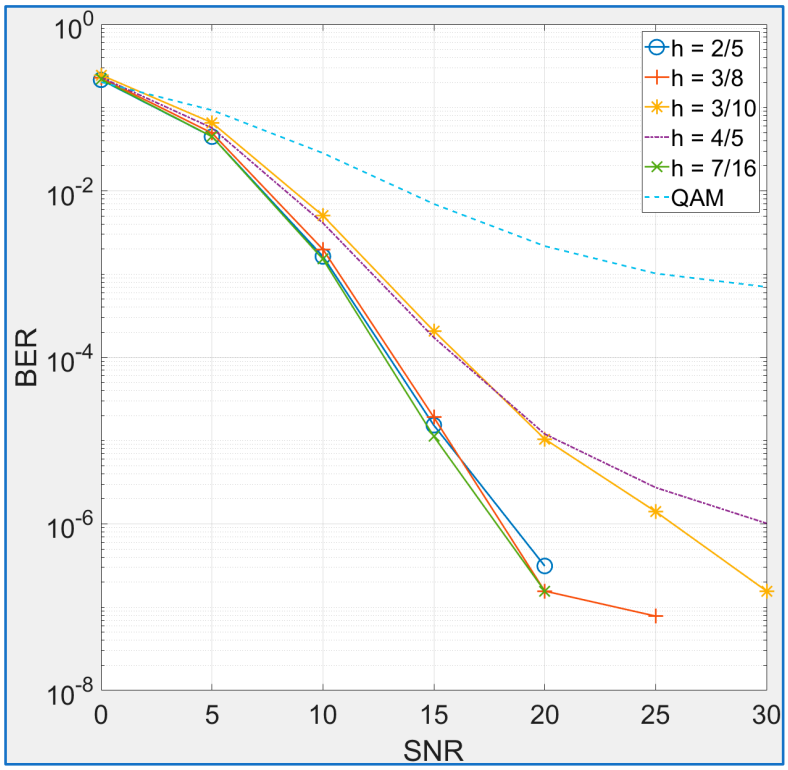

Figure 14. BER performance of CPM-GFDM vs. QAM-GFDM with $J = 4$ for matched filter receiver over frequency-selective channels.

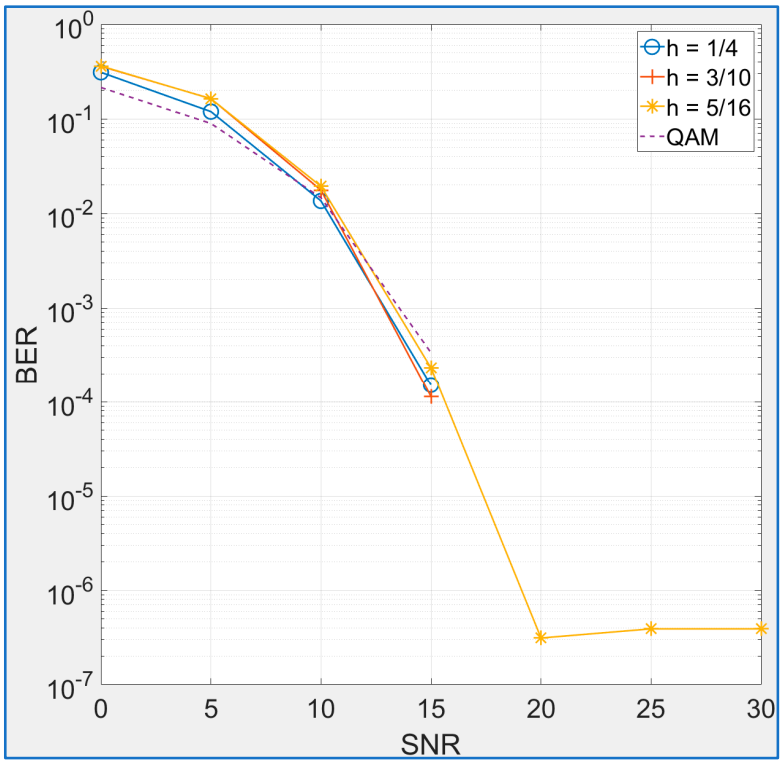

Figure 15. BER performance of CPM-GFDM v.s QAM-GFDM with $J = 4$ for zero forcing receiver over frequency-selective channels.

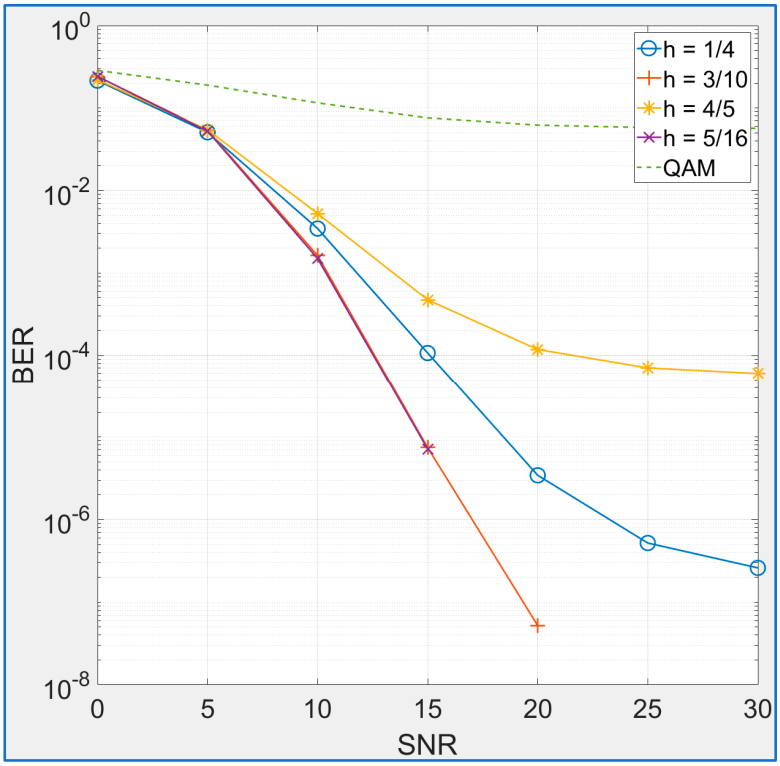

Figure 16. BER performance of CPM-GFDM vs. QAM-GFDM with $J = 8$ for matched filter receiver over frequency-selective channels.

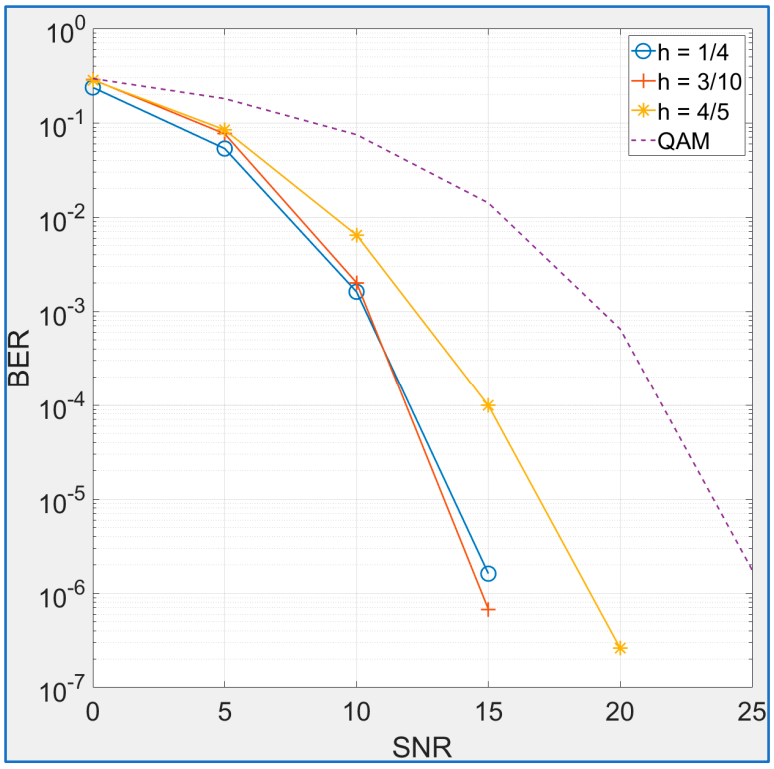

Figure 17. BER performance of CPM-GFDM vs. QAM-GFDM with $J = 8$ for zero forcing receiver over frequency-selective channels.

The error performance of CPM-GFDM against QAM-GFDM with $J = 4$ is shown in Figures 14 and 15 for the two receivers. For the case of the matched filter receiver, there are five values of h for which the error performance of the proposed system is better than QAM-GFDM. The best performance is observed in the case when $h = 7/16$. The complete list of h values for which the proposed system outperforms QAM-GFDM is given in Table 4. When using a zero-forcing receiver, there are three values of h that perform better than QAM-GFDM. However, at high SNR values, $h = 3/10$ gives the best performance.

Figures 16 and 17 depict the error performance with $J = 8$. It is observed that, in this case, there are four values of h that outperform conventional GFDM when using a matched filter receiver. The best performance is observed in the case when $h = 5/16$ and $h = 3/10$. Furthermore, it is noted in Figure 17 that, when using zero forcing receiver, the proposed system outperforms the conventional GFDM for three values of h, i.e., $h = 1/4$, $h = 3/10$ and $h = 4/5$, with the best performance observed in the case of $h = 3/10$.

4. Discussion

From the results presented in the previous two sections, it is noted that the proposed CPM-GFDM always performs better than conventional GFDM for several values of modulation index h when using a matched filter receiver. In the case of a zero-forcing receiver, only when $J = 8$ are there modulation indices that perform better than conventional GFDM if the channel is AWGN. When the channel is frequency-selective, the number of h values that outperform conventional GFDM are much less than those for the AWGN channel. However, unlike for the AWGN channel, for $J = 4$ there are values of h that perform better than conventional GFDM. In the case of the AWGN channel, the best performing modulation indices are $1/2$, $3/10$ (appearing twice), $5/16$ (appearing twice), and $7/16$, as is evident from Table 4, while in the case of frequency-selective channels, the best performing modulation indices are $3/10$ (appearing thrice), $5/16$ and $7/16$ (appearing twice), as has been shown in Table 4. Finally, it can be concluded that the proposed CPM-GFDM configuration outperforms conventional GFDM.

5. Conclusions

A novel scheme, CPM-GFDM, has been introduced for frequency-selective wireless channels. In this scheme, the memoryless mapping schemes such as QAM and PSK are replaced with CPM mapping that has memory. At the GFDM receiver, this memory is exploited to improve the error performance of the CPM-GFDM scheme. Using extensive simulations and two types of receivers, i.e., matched filter and zero-forcing, it has been shown that there are several values of the modulation index h for which the proposed CPM-GFDM system outperforms the conventional GFDM system. The performance of the proposed system is particularly better than a conventional scheme when using higher modulation schemes, i.e., when sending two bits or three bits at a time. Hence, the proposed scheme is a strong candidate for high-speed wireless communication.

Funding: The author would like to thank the Deanship of Scientific Research at Umm Al-Qura University for supporting this work by Grant Code: (22UQU4300148DSR02).

Institutional Review Board Statement: Not applicable.

Informed Consent Statement: Not applicable.

Data Availability Statement: Not applicable.

Acknowledgments: The author would like to thank the Deanship of Scientific Research at Umm Al-Qura University for supporting this work by Grant Code: (22UQU4300148DSR02). The author would also like to thank the College of Computer and Information Systems, Umm Al-Qura University, Makkah, Saudi Arabia.

Conflicts of Interest: The author declares no conflict of interest.

References

1. Schaich, F.; Wild, T. Waveform Contenders for 5g—OFDM Vs. FBMC Vs. UFMC. In Proceedings of the 2014 6th International Symposium on Communications, Control and Signal Processing (ISCCSP), Athens, Greece, 21–23 May 2014.
2. Bellanger, M.; Le Ruyet, D.; Roviras, D.; Terré, M.; Nossek, J.; Baltar, L.; Bai, Q.; Waldhauser, D.; Renfors, M.; Ihalainen, T. Fbmc Physical Layer: A Primer. *PHYDYAS* **2010**, *25*, 7–10.
3. Shawqi, F.S.; Audah, L.; Mostafa, S.A.; Gunasekaran, S.S.; Baz, A.; Hammoodi, A.T.; Alhakami, H.; Hassan, M.H.; Jubair, M.; Alhakami, W. A New SLM-UFMC Model for Universal Filtered Multi-Carrier to Reduce Cubic Metric and Peak to Average Power Ratio in 5g Technology. *Symmetry* **2020**, *12*, 909. [CrossRef]
4. Ahmed, M.A.; Baz, A.; Tsimenidis, C.C. Performance Analysis of Noma Systems over Rayleigh Fading Channels with Successive-Interference Cancellation. *IET Commun.* **2020**, *14*, 1065–1072. [CrossRef]
5. Saito, Y.; Kishiyama, Y.; Benjebbour, A.; Nakamura, T.; Li, A.; Higuchi, K. Non-Orthogonal Multiple Access (NOMA) for Cellular Future Radio Access. In Proceedings of the 2013 IEEE 77th Vehicular Technology Conference (VTC Spring), Dresden, Germany, 2–5 June 2013.
6. Abdoli, J.; Jia, M.; Ma, J. Filtered OFDM: A New Waveform for Future Wireless Systems. In Proceedings of the 2015 IEEE 16th International Workshop on Signal Processing Advances in Wireless Communications (SPAWC), Stockholm, Sweden, 28 June–1 July 2015.
7. Fettweis, G.; Krondorf, M.; Bittner, S. GFDM-Generalized Frequency Division Multiplexing. In Proceedings of the VTC Spring 2009-IEEE 69th Vehicular Technology Conference, Barcelona, Spain, 26–29 April 2009.
8. Li, Y.; Niu, K.; Dong, C. Polar-Coded GFDM Systems. *IEEE Access* **2019**, *7*, 149299–149307. [CrossRef]
9. Ahamad, R.Z.; Javed, A.R.; Mehmood, S.; Khan, M.Z.; Noorwali, A.; Rizwan, M. Interference Mitigation in D2D Communication Underlying Cellular Networks: Towards Green Energy. *CMC-Comput. Mater. Contin.* **2021**, *68*, 45–58. [CrossRef]
10. Zhong, J.; Chen, G.; Mao, J.; Dang, S.; Xiao, P. Iterative Frequency Domain Equalization for MIMO-GFDM Systems. *IEEE Access* **2018**, *6*, 19386–19395. [CrossRef]
11. Matthé, M.; Mendes, L.; Gaspar, I.; Michailow, N.; Zhang, D.; Fettweis, G. Precoded GFDM Transceiver with Low Complexity Time Domain Processing. *EURASIP J. Wirel. Commun. Netw.* **2016**, *2016*, 1–9. [CrossRef]
12. Michailow, N.; Mendes, L.; Matthé, M.; Gaspar, I.; Festag, A.; Fettweis, G. Robust WHT- GFDM for the Next Generation of Wireless Networks. *IEEE Commun. Lett.* **2014**, *19*, 106–109. [CrossRef]
13. Farhang, A.; Marchetti, N.; Doyle, L.E. Low-Complexity Modem Design for GFDM. *IEEE Trans. Signal Process.* **2015**, *64*, 1507–1518. [CrossRef]
14. Gaspar, I.; Michailow, N.; Navarro, A.; Ohlmer, E.; Krone, S.; Fettweis, G. Low Complexity GFDM Receiver Based on Sparse Frequency Domain Processing. In Proceedings of the 2013 IEEE 77th Vehicular Technology Conference (VTC Spring), Dresden, Germany, 2–5 June 2013.
15. Datta, R.; Michailow, N.; Lentmaier, M.; Fettweis, G. GFDM Interference Cancellation for Flexible Cognitive Radio Phy Design. In Proceedings of the 2012 IEEE Vehicular Technology Conference (VTC Fall), Quebec City, QC, Canada, 3–6 September 2012.
16. Chen, P.-C.; Su, B.; Huang, Y. Matrix Characterization for GFDM: Low Complexity Mmse Receivers and Optimal Filters. *IEEE Trans. Signal Process.* **2017**, *65*, 4940–4955. [CrossRef]
17. Matthé, M.; Zhang, D.; Fettweis, G. Low-Complexity Iterative MMSE-Pic Detection for MIMO- GFDM. *IEEE Trans. Commun.* **2017**, *66*, 1467–1480. [CrossRef]
18. Maraş, M.; Ayvaz, E.N.; Gömeç, M.; Savaşcıhabeş, A.; Özen, A. A Novel GFDM Waveform Design Based on Cascaded WHT-LWT Transform for the Beyond 5g Wireless Communications. *Sensors* **2021**, *21*, 1831. [CrossRef] [PubMed]
19. Wang, Z.; Mei, L.; Sha, X. Ber Analysis for GFDM Systems with Gabor Mmse Receiver. *IEEE Commun. Lett.* **2018**, *22*, 2222–2225. [CrossRef]
20. Wang, Z.; Mei, L.; Sha, X.; Leung, V.C.M. Ber Analysis of Wfrft Precoded OFDM and GFDM Waveforms with an Integer Time Offset. *IEEE Trans. Veh. Technol.* **2018**, *67*, 9097–9111. [CrossRef]
21. Carrillo, D.; Kumar, S.; Fraidenraich, G.; Mendes, L.L. Bit Error Probability for Mmse Receiver in GFDM Systems. *IEEE Commun. Lett.* **2018**, *22*, 942–945. [CrossRef]
22. Wang, Y.; Fortier, P. Performance Analysis of Ldpc Coded GFDM Systems. *IET Commun.* **2022**, *16*, 1663–1673. [CrossRef]
23. Wang, H.-F.; Ueng, F.-B.; Chiang, C.-T. High Spectral Efficiency and Low Error Rate MIMO-GFDM for Next-Generation Communication Systems. *IEEE Trans. Veh. Technol.* **2021**, *71*, 503–517. [CrossRef]
24. Wang, H.-F.; Ueng, F.-B.; Shen, Y.-S.; Lin, K.-X. Low-Complexity Receivers for Massive MIMO-GFDM Communications. *Trans. Emerg. Telecommun. Technol.* **2021**, *32*, e4219. [CrossRef]
25. Wang, H.-F.; Ueng, F.-B.; Sung, Y.-H. Low-Complexity Mu-MIMO-GFDM Joint Receivers. *Int. J. Electron.* **2022**, *110*, 1–22. [CrossRef]
26. Wang, Y.; Fortier, P. Polynomial Expansion-Based Mmse Channel Estimation and Precoding for Massive MIMO-GFDM Systems. *Wirel. Pers. Commun.* **2022**, *127*, 1–21. [CrossRef]
27. Wang, Y.; Fortier, P. Union Bound on the Bit Error Rate for MIMO-GFDM Systems. *Wirel. Pers. Commun.* **2022**, *123*, 1825–1839. [CrossRef]
28. Kassam, J.; Miri, M.; Magueta, R.; Castanheira, D.; Pedrosa, P.; Silva, A.; Dinis, R.; Gameiro, A. Two-Step Multiuser Equalization for Hybrid mmwave Massive MIMO GFDM Systems. *Electronics* **2020**, *9*, 1220. [CrossRef]

29. Li, S.; Zhao, Y.; He, L.; Wu, Z.; Li, Y. Design and Performance Analysis of a GFDM-DCSK Communication System. In Proceedings of the 2016 13th IEEE Annual Consumer Communications & Networking Conference (CCNC), Las Vegas, NV, USA, 9–12 January 2016.
30. Aulin, T.; Sundberg, C.-E. Bounds on the Performance of Binary Cpfsk Type of Signaling with Input Data Symbol Pulse Shaping. In Proceedings of the NTC'78, National Telecommunications Conference, Birmingham, AL, USA, 3–6 December 1978; Volume 1.
31. Aulin, T.; Sundberg, C. Continuous Phase Modulation-Part I: Full Response Signaling. *IEEE Trans. Commun.* **1981**, *29*, 196–209. [CrossRef]
32. Aulin, T.; Rydbeck, N.; Sundberg, C.-E. Continuous Phase Modulation-Part II: Partial Response Signaling. *IEEE Trans. Commun.* **1981**, *29*, 210–225. [CrossRef]
33. Sun, Y. Optimal Parameter Design of Continuous Phase Modulation for Future Gnss Signals. *IEEE Access* **2021**, *9*, 58487–58502. [CrossRef]
34. Imran, M.; Rashid, M.; Jafri, A.R.; Najam-ul-Islam, M. Acryp-Proc: Flexible Asymmetric Crypto Processor for Point Multiplication. *IEEE Access* **2018**, *6*, 22778–22793. [CrossRef]
35. Rashid, M.; Imran, M.; Jafri, A.R.; Al-Somani, T.F. Flexible Architectures for Cryptographic Algorithms—A Systematic Literature Review. *J. Circuits Syst. Comput.* **2019**, *28*, 1930003. [CrossRef]
36. Alves, B.M.; Mendes, L.L.; Guimaraes, D.A.; Gaspar, I.S. Performance of GFDM over Frequency-Selective Channels. In Proceedings of the International Workshop on Telecommunications, Santa Rita do Sapuca, Brazil, 2–4 July 2013.
37. Proakis, J.G.; Salehi, M. *Digital Communications*; McGraw-Hill: New York, NY, USA, 2008.
38. Tasadduq, I.A.; Rao, R.K. OFDM-CPM Signals. *Electron. Lett.* **2002**, *38*, 80–81. [CrossRef]
39. Anderson, J.B.; Aulin, T. *Digital Phase Modulation*; Plenum: New York, NY, USA, 1986.
40. Matthe, M.; Michailow, N.; Gaspar, I.; Fettweis, G. Influence of Pulse Shaping on Bit Error Rate Performance and out of Band Radiation of Generalized Frequency Division Multiplexing. In Proceedings of the 2014 IEEE International Conference on Communications Workshops (ICC), Sydney, Australia, 10–14 June 2014.
41. Das, S.S.; Tiwari, S. Discrete Fourier Transform Spreading-Based Generalised Frequency Division Multiplexing. *Electron. Lett.* **2015**, *51*, 789–791. [CrossRef]
42. Michailow, N.; Matthe, M.; Gaspar, I.S.; Caldevilla, A.N.; Mendes, L.L.; Festag, A.; Fettweis, G. Generalized Frequency Division Multiplexing for 5th Generation Cellular Networks. *IEEE Trans. Commun.* **2014**, *62*, 3045–3061. [CrossRef]
43. Tasadduq, I.A.; Rao, R.K. OFDM-CPM Signals for Wireless Communications. *Can. J. Electr. Comput. Eng.* **2003**, *28*, 19–25. [CrossRef]
44. Sklar, B. *Digital Communications: Fundamentals and Applications*, 2nd ed.; Prentice-Hall: Englewood Cliffs, NJ, USA, 2001.
45. Haykin, S. *Communication Systems*; John Wiley & Sons: Hoboken, NJ, USA, 2008.
46. Vodafone Chair Mobile Communications Systems—Testbed. Available online: http://owl.ifn.et.tu-dresden.de/GFDM/ (accessed on 3 January 2023).
47. Üçüncü, A.B.; Yilmazx, A.Ö. Out-of-Band Radiation Comparison of GFDM, WCP-COQAM and OFDM at Equal Spectral Efficiency. *arXiv* **2015**, arXiv:1510.01201.
48. Behrouz, F.-B. OFDM Versus Filter Bank Multicarrier. *IEEE Signal Process. Mag.* **2011**, *28*, 92–112.
49. Sim, Z.A.; Juwono, F.H.; Reine, R.; Zang, Z.; Gopal, L. Performance of GFDM Systems Using Quadratic Programming Pulse Shaping Filter Design. *IEEE Access* **2020**, *8*, 37134–37146. [CrossRef]
50. Michailow, N.; Datta, R.; Krone, S.; Lentmaier, M.; Fettweis, G. Generalized Frequency Division Multiplexing: A Flexible Multi-Carrier Modulation Scheme for 5th Generation Cellular Networks. In Proceedings of the German Microwave Conference (GeMiC), Ilmenau, Germany, 12–14 March 2012.
51. Murad, M.; Tasadduq, I.A.; Otero, P. Towards Multicarrier Waveforms Beyond OFDM: Performance Analysis of GFDM Modulation for Underwater Acoustic Channels. *IEEE Access* **2020**, *8*, 222782–222799. [CrossRef]
52. Li, W.; Lilleberg, J.; Rikkinen, K. On Rate Region Analysis of Half-and Full-Duplex OFDM Communication Links. *IEEE J. Sel. Areas Commun.* **2014**, *32*, 1688–1698. [CrossRef]